Growth of Mesoporous Materials within Colloidal Crystal Films by Spin-Coating

Luis A. Villaescusa,[†] Agustín Mihi,[‡] Isabel Rodríguez,[†] Alfonso E. García-Bennett,[§] and Hernán Míguez*[,‡]

Departamento de Química y Centro Tecnológico de Ondas, Universidad Politécnica de Valencia, Camino de Vera s/n, 46022 Valencia, Spain, Instituto de Ciencia de Materiales de Sevilla, Consejo Superior de Investigaciones Científicas, Avda. Américo Vespucio s/n, 41092 Sevilla, Spain, and Structural Chemistry, Arrhenius Laboratory, Stockholm University, S-10691 Stockholm, Sweden

Received: June 28, 2005; In Final Form: August 28, 2005

A combination of colloidal crystal planarization, stabilization, and novel infiltration techniques is used to build a bimodal porous silica film showing order at both the micron and the nanometer length scale. An infiltration method based on the spin-coating of the mesophase precursor onto a three-dimensional polystyrene colloidal crystal film allows a nanometer control tuning of the filling fraction of the mesoporous phase while preserving the optical quality of the template. These materials combine a high specific surface arising from the nanopores with increased mass transport and photonic crystal properties provided by the order of the macropores. Optical Bragg diffraction from these type of hierarchically ordered oxides is observed, allowing performing of optical monitoring of the different processes involved in the formation of the bimodal silica structure.

Introduction

Materials in which networks of pores of different dimensions are interwoven bestow the possibility to combine the different functionality provided by each type of porosity. For instance, a structure of interconnected macropores whose walls possess finer pores would present increased mass transport through the former and high specific surface area due to the latter.[1] The fabrication of such kinds of materials has been mainly motivated by the potential applications in fields as diverse as chromatography, biomaterials, or catalysis. On the other hand, in the context of photonic materials, periodic structuring with lattice parameters on the order of a micrometer has been employed to endow with color otherwise transparent materials.[2] This color results from the Bragg diffraction occurring within periodic dielectrics, also known as photonic crystals, and can be tuned by varying either the lattice parameter or its composition.[3] In this communication, we show how to build films of ordered spherical macrocavities possessing mesoporous walls and displaying photonic crystal properties, which can be accurately determined with a precision on the order of a few nanometers. We combine crystallization of polystyrene colloids into films through self-assembly with a mesoporous infiltration technique that is compatible with current microelectronics or microphotonics chip-processing technology. Large mesoporous films displaying intense visible colors resulting from the Bragg diffraction caused by the ordering of the macroporous cavities are realized. These films combine the optical functionality and high pore accessibility arising from a macroporous lattice, with high specific surface area, reactivity, and size selectivity characteristics of a mesoporous network.

Since the seminal work by P. Yang et al.,[4] several methods to build hierarchical materials showing simultaneously ordered pores at the micron and the nanometer length scale have been developed. Some are based on the infiltration of a gel precursor, typically made of a self-organized surfactant molecular network around which amorphous or crystalline silica forms, within the voids of close-packed polystyrene colloidal particles.[5−8] Once the gel is cured, both the colloidal and the surfactant organic templates are removed by calcination to yield macroporous lattices within mesoporous backgrounds. Also, three-dimensional arrangements of large hollow spherical zeolite shells have been synthesized by hydrothermal treatment of preseeded ordered mesoporous silica spheres.[9] Other attempts use the synthesis of mesoporous colloidal spheres within a void and a periodic polymer matrix,[10] achieving a lattice composed of mesoporous spheres instead of cavities. Very recently, channels of molecular dimensions have been grown within semi-ordered tubular macroporous alumina.[11] However, none of these approaches yielded optically functional materials. The reason for this lack of optical quality is, very likely, twofold: the absence of long-range order of the original colloidal packing used as scaffold and the presence of imperfections introduced during the sol−gel precursor infiltration, curing, and porogen removal process. Furthermore, no control over the filling fraction of the meso- or microporous guest material is possible by the infiltration methods so far employed, which prevents the precise tuning of the optical properties in the desired light wavelength range. Here, we demonstrate that imposing controlled optical functionality to a mesoporous network is possible by combining colloidal self-organization with spin-coating infiltration of a mesoporous gel precursor. This route enables a controlled infiltration of the mesoporous network without disrupting the long-range order of the planarized colloidal lattice, overcoming the limitations mentioned above.

Experimental Section

Colloidal Crystal Film Preparation. We begin by depositing a colloidal crystal film on top of a glass substrate by letting a suspension of polystyrene microspheres (average particle di-

* Corresponding author. E-mail: hernan@icmse.csic.es.
[†] Departamento de Química y Centro Tecnológico de Ondas.
[‡] Instituto de Ciencia de Materiales de Sevilla.
[§] Structural Chemistry, Arrhenius Laboratory.

10.1021/jp053511m CCC: $30.25
Published on Web 10/01/2005

ameters ranging from 300 to 600 nm) in ethanol to evaporate while the substrate is vertically placed in the beaker. Convection and capillary forces acting on the particles at the meniscus between the substrate surface and the suspension give rise to highly crystalline films.[12] Polystyrene colloidal spheres were purchased from IKERLAT Polymers. Glass microscope slides were used as substrates. Prior to colloidal crystallization, they were cleaned with distilled water and acetone and then ultrasonicated for 30 min in carbon tetrachloride. After this, they were washed with 2-propanol, distilled water, and then ultrasonicated in a mixture of 4:1 H_2SO_4 (98%)/H_2O_2 (32% aqueous solution). Finally, the substrates were copiously washed with distilled deionized water and dried with a stream of nitrogen. Polystyrene colloidal suspensions employed during the crystallization process had a concentration of 1 wt % in ethanol. Suspensions were allowed to settle on a vibration-free table until a large area ($\sim cm^2$) of the substrate was covered with a colored bright coating.

Mechanical Stabilization of Colloidal Crystals. Prior to infiltration, some of the films were mechanically stabilized by growing a thin layer of dense silica using a chemical vapor deposition (CVD) process.[13] The reactants employed were $SiCl_4$ (99%, Sigma-Aldrich) and distilled water. They were kept in bubblers through which a N_2 flow passed alternately, carrying them to the cell in which the colloidal crystal film was placed. N_2 flows employed were 50 mL/min for each reactant. The deposition line was cleaned between treatments using a similar flow of pure N_2. Only one deposition cycle of each reactant was enough to mechanically stabilize the crystals, leaving their external pores still open. Both CVD stabilized and nonstabilized films were employed as starting materials.

Mesoporous Gel Precursor Preparation. A mesoporous sol−gel precursor was prepared by following a similar procedure to that previously reported to attain continuous mesoporous films.[14] Pluronic F-127, a triblock copolymer, was used as a structuring agent to yield a hybrid organic−inorganic mesoporous network. Different solutions were derived by dilution with ethanol of this parent gel. A solution containing 8.83 g of ethanol, 0.69 g of water and 0.1 g of a 1 M HCl aqueous solution was first prepared. Pluronic F-127 (0.46 g) (Sigma-Aldrich) was then added under stirring until a clear solution was formed. Finally, 1.0 g of TEOS (98%, Merck) was then added dropwise under stirring. The solution was then stirred at 80 °C for 1 h in a flask provided with a condenser. Overall molar gel composition was 1 TEOS: 9.2 H_2O: 0.02 HCl: 40 EtOH: 7.2×10^{-3} Pluronic F127.

Spin-Coating Infiltration. Freshly prepared mesoporous precursor solutions were infiltrated within the sphere network by means of a spin-coater (Novocontrol SCI-50). As in a standard spin-coating process, a drop of a solution of the mesoporous precursor (15−30 μL) was dropped onto the colloidal crystal film while spinning at high speed (in our case, between 20 and 60 rps). The substrate was allowed to spin for 2 min. This process was repeated as many times as necessary to attain the desired degree of infiltration. This technique, which we will refer as spin-coating infiltration (SCI) in what follows, allows for a homogeneous infiltration of the void volume of the colloidal crystal films (typically, with a surface of a few squared centimeters and a thickness of a few microns). More specifically, the infiltration of the films whose results are herein presented were performed using a 2-fold diluted solution of the aforementioned parent gel in ethanol, except for those cases explicitly indicated in the text. After each infiltration process, the film was allowed to dry for 10 min in an oven at 70 °C. The infiltrated films were then allowed to cure in an oven at 70 °C for 21 days in order to increase the connectivity of the mesoporous network.

Porogen Removal. Finally, the original polystyrene sphere crystal was dissolved by placing the infiltrated film in toluene at room temperature for 1 day and, afterward, in a Soxhlet extractor containing toluene overnight to ensure complete elimination of the matrix, leaving large spherical cavities in the films. To eliminate the surfactant used as template for the mesophase, the polystyrene-free films were left overnight in the same extractor containing ethanol. Removal of both types of organic porogens was monitored and confirmed by infrared transmission spectroscopy.

Electron Microscope Characterization. Scanning electron microscopy (SEM) was performed with a JEOL-JSM6300 operating at 20 keV. Cleaved edges of films were sputtered with a thin layer of gold (sputter coater Baltec SCD005) before introducing them in the microscope sample chamber. Transmission electron microscopy (TEM) was carried out with a JEOL-3010 microscope operating at 300 kV (Cs 0.6 mm, resolution 1.7 Å). Images were recorded using a CCD camera (model Keen View, SIS analysis, size 1024 × 1024, pixel size 23.5 μm × 23.5 μm) at 4000−100000× magnification using low-dose conditions. Samples for TEM analysis were prepared by carefully scratching the film onto a mortar, where they were crushed before depositing them onto holey carbon films supported on a Cu TEM grid.

Optical Spectroscopy. Optical characterization was performed using a Fourier transform infrared spectrophotometer (Bruker IFS-66) attached to a microscope and operating in reflection mode. A ×4 objective with a numerical aperture of 0.1 (light cone angle ±5.7°) was used to irradiate the sample and collect the reflected light at quasinormal incidence with respect to the (111) planes of the colloidal lattice. A spatial filter was used to selectively detect light from 0.1 mm^2 circular regions of the sample.

Results and Discussion

Scanning electron microscopy (SEM) and high resolution transmission electron microscopy (HRTEM) analysis were performed to determine the structural and morphological features of the resulting films. Figures 1 and 2 show some images of bimodal structures attained using as-grown and dense silica CVD stabilized polystyrene sphere crystals as templates, respectively. Typically, the thickness of films such as those shown in Figures 1a and 2a can be varied between 1 and 10 μm. Both types of films present good mechanical stability, although those made from nonstabilized crystals present more cracks arising from shrinkage of the structure occurring mainly during removal of both types of porogen templates. The bimodal character of the films can be clearly appreciated in Figure 1b and c, in which macroporous and mesoporous order can be simultaneously observed. Figure 1d shows a hexagonal arrangement of mesopores parallel to the incident beam direction, resembling that of MCM-41 or SBA-type structures. The skeleton of the hierarchical structure is thus made of mesoporous silica channels (unit cell parameter 9.5 nm after Fourier transform diffractograms and contrast profile curves, estimated pore size 6 nm) surrounding macroscopic size pores (average pore diameter 375 nm) ordered in a face-centered cubic (fcc) lattice. Large circular windows (average diameter 60 nm) interconnect the macropores and provide increased mass transport through the structure. In

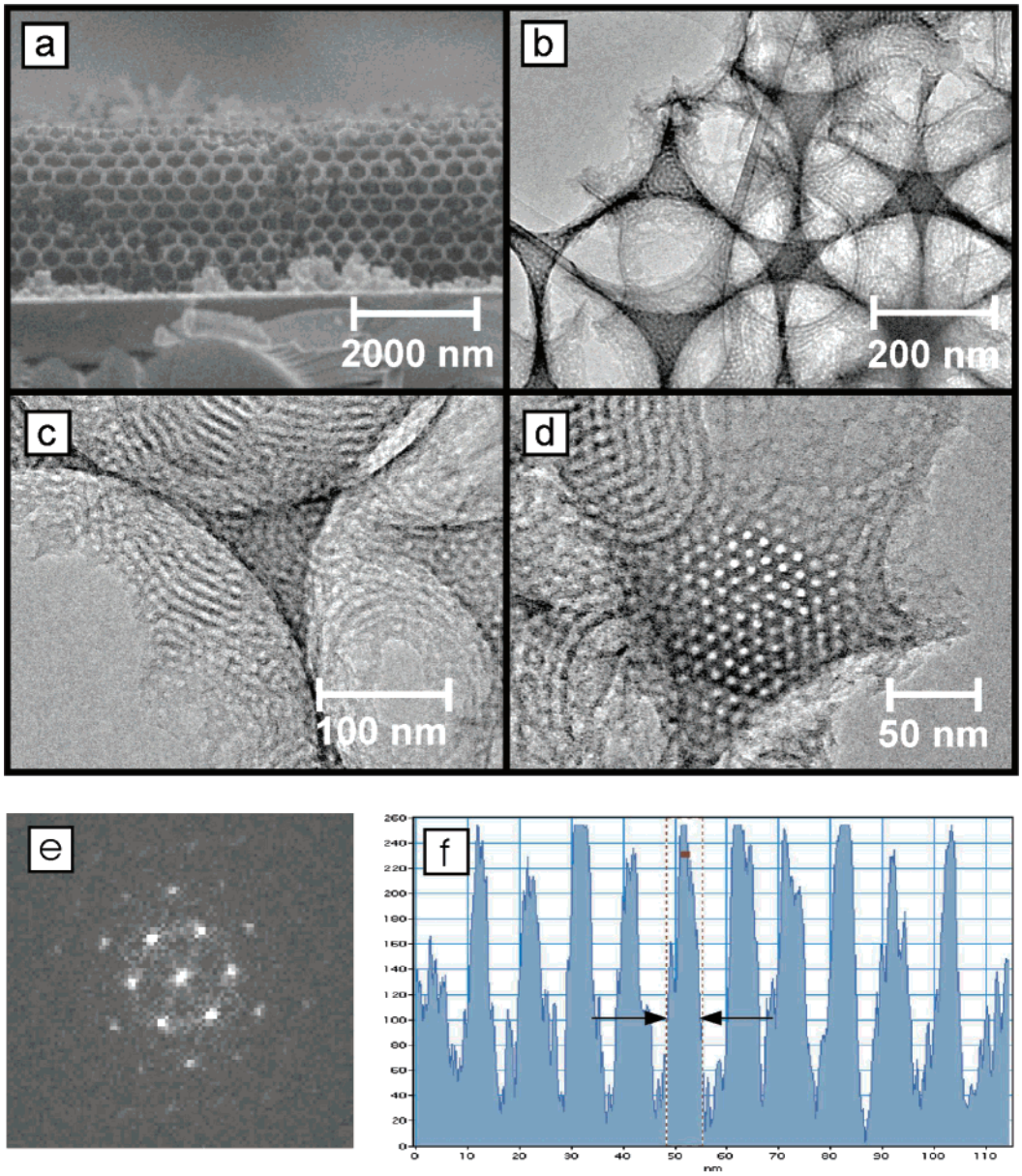

Figure 1. (a) SEM image of a cross section of a three-dimensionally ordered macroporous cavity film built on top of a glass substrate by the method herein reported. Pictures shown in (b), (c), and (d) correspond to HRTEM images of a thin piece of the same film: (b) A top view of a stacking of (111) planes of the macroporous fcc lattice. (c) A closer look at the cavity walls reveals their ordered mesoporous structure, several lattice planes being clearly distinguished. (d) Hexagonal arrangement of the tubular mesophase observed in the macropore walls. The unit cell parameter could be accurately calculated from Fourier transform (FT) diffractograms such as those shown in (e) on the basis of a hexagonal unit cell with spacegroup symmetry *p6mm*. The result was consistent with pore size estimations attained from contrast profile curves such as that shown in (f), plotted along a line crossing the equator of the ordered mesopores.

the case of samples made from silica-stabilized polystyrene templates, the mesoporous material is deposited on top of a thin layer of dense silica. Figure 2c and d display images of dense silica spherical shells without and with mesoporous coating, respectively. Images such as the one displayed in Figure 2b confirm the ordering of the pores at both the macro- and the mesoscale levels also for silica-stabilized structures. For dilute precursor solutions, a very fine control over the amount of infiltrated material is attained by SCI. As a result of the spinning, the mesoporous precursor is spread over the sphere surface, and good ordering at the mesoscale is found along with highly uniform coatings. However, it should be noticed that using very dilute solutions could give rise to incomplete, nonuniform, coverage of the sphere surface, yielding disordered mesoporous backbones. HRTEM micrographs displayed in Figure 2a−d correspond to ordered mesoporous wall colloidal crystal films obtained after performing two infiltrations of a 2-fold diluted solution of the aforementioned precursor gel, while Figure 2e and f show disordered mesoporous walls attained after eight infiltrations of a 5-fold diluted solution of the same gel.

Optical spectroscopy is a suitable nondestructive method to monitor the entire preparation process of the bimodal material because any change of the composition or geometry of the lattice affects the photonic crystal properties of the film. Figure 3a shows the specular reflectance spectra of a polystyrene colloidal crystal (average sphere diameter 545 nm) as grown (red line) and after subsequent infiltration with the mesoporous precursor. The main reflectance peak in the original structure is the result of the interference of the light beams scattered at each close-packed (111) sphere crystal plane parallel to the substrate, while secondary lobes arise from interference of the beams reflected at the top and bottom surface of the film. Each time the

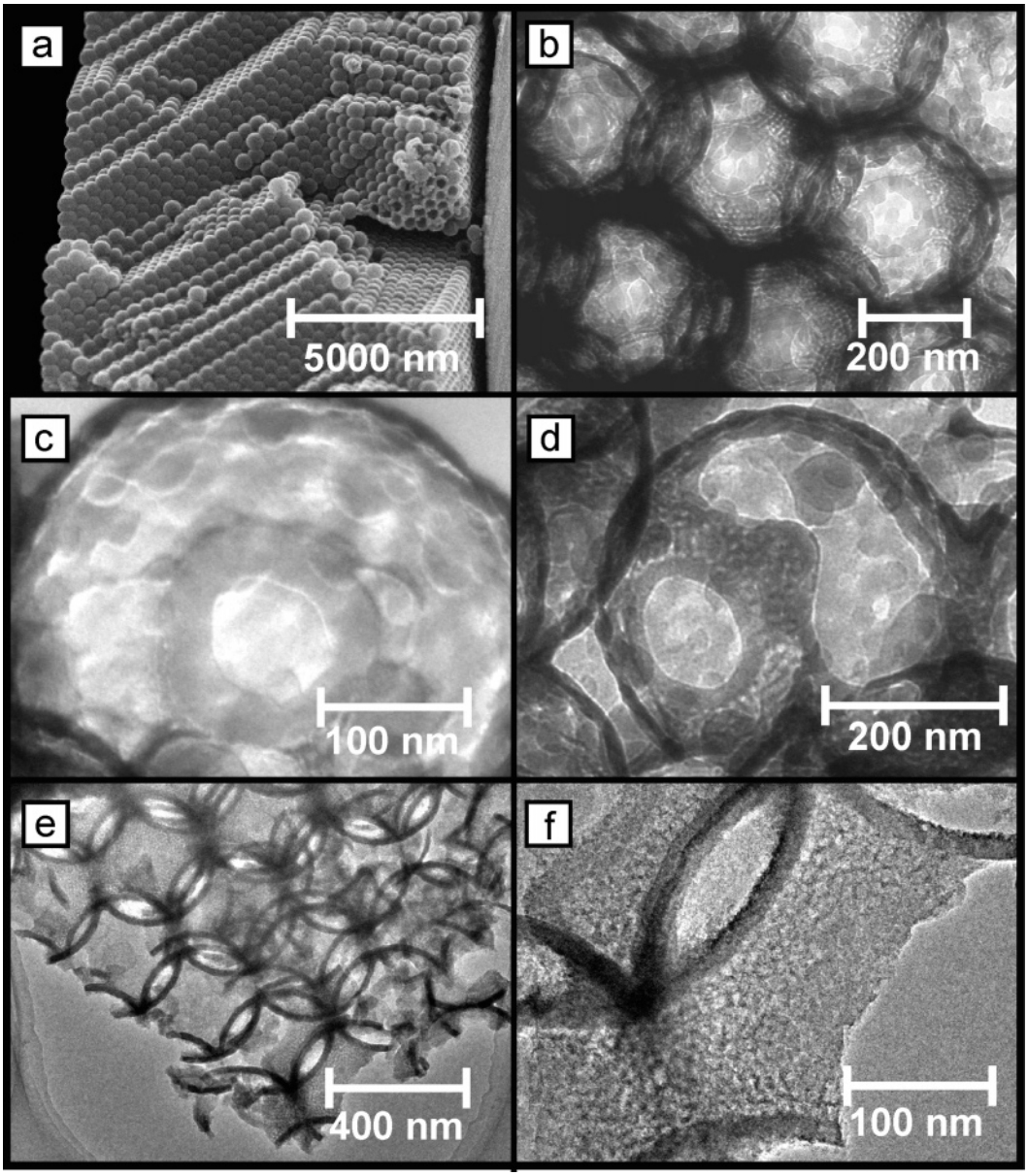

Figure 2. (a) SEM image of a cross section of a macroporous cavity film made from a silica-stabilized polystyrene sphere crystal. (b), (c), and (d) are HRTEM images of a thin piece of the same film. (b) Picture showing, simultaneously, the order at the macropore and the mesopore level. (c) An example of the stabilizing dense silica shell on top of which the mesoporous network is built up by infiltration. For the sake of clarity, the polystyrene sphere used as a template has been dissolved to show only the shell. (d) Mesoporous network on top of dense silica spherical shells. The circular windows interconnecting the macropores can be clearly seen. Images shown in panels (e) and (f) correspond to a disordered mesoporous network built in a macroporous lattice of dense silica shells. The different density of both kinds of silica can be clearly appreciated.

mesoporous precursor is deposited onto the polystyrene spheres by SCI, it causes a red-shift of the Bragg reflection maximum. In a first approximation, the maximum spectral position $\lambda_{(111)}$ is given by:

$$\lambda_{(111)} = 2 \cdot d_{(111)} \cdot \sqrt{\langle \epsilon \rangle} \tag{1}$$

an expression in which Bragg's and Snell's laws are combined and in which $d_{(111)}$ is the interplanar distance along the [111] direction and $\langle \epsilon \rangle$ is the volume-averaged dielectric constant of the composite:

$$\langle \epsilon \rangle = \sum_i ff_i \cdot \epsilon_i \tag{2}$$

where ff_i and ϵ_i are the filling fraction and dielectric constant of each component of the structure. It can be clearly seen from eq 1 that an increase in the filling fraction of the mesoporous precursor would cause a shift of the Bragg reflection toward higher wavelengths, as observed in Figure 3. We have fitted these spectra using a scalar wave approximation,[15] in which both the crystal thickness and the substrate are taken into account, to estimate the changes in the mesoporous precursor filling fraction at each step of the infiltration process. Results are shown in the inset in Figure 3a. Conversely, curing the mesoporous precursor, dissolving the polystyrene spheres, and extracting the surfactant imply lowering the average refractive index of the composite and therefore give rise to three subsequent blue-shifts of the Bragg reflection, as shown in Figure 3b. In this example, we start from a mesoporous precursor infiltrated polystyrene sphere film (particle diameter 360 nm), which displayed a clear reflection maximum in the near-infrared. After curing, we observe a small shift of the peak that can be attributed to the loss of water originally trapped within the mesoporous network

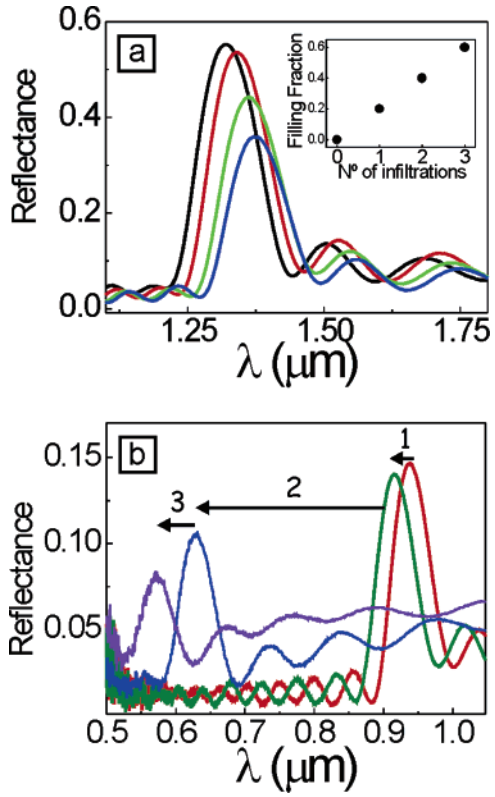

Figure 3. Specular optical reflectance spectra of a colloidal photonic crystal film at different stages of the mesoporous precursor infiltration, curing, and porogen template removal process. (a) Reflectance of a colloidal photonic crystal film made of 545 nm average diameter spheres before (black line) and after one (red line), two (green line), and three (blue line) consecutive infiltrations of the mesoporous precursor. Inset shows the evolution of the mesoporous filling fraction of the pore volume for this particular infiltration process as estimated from the fittings of the optical data. (b) Reflectance spectra of a 360 nm average diameter sphere crystal infiltrated with mesoporous precursor (red line), and after curing the precursor (green line), removal of the polystyrene template in toluene (blue line), and extraction of the surfactant in ethanol (violet line). Arrows and numbers drawn over them indicate the direction of the shift and the order in which they take place, respectively.

or generated by silanol condensation. Etching of the polystyrene sphere template in toluene and extraction of the surfactant from the mesoporous walls with ethanol are responsible for the two final shifts. Shrinkage of the structure was also observed by electron microscopy and also contributes to this change. An estimation of the magnitude of the average shrinkage could be attained from the fitting of the optical reflectance spectra. No significant change in the colloidal crystal lattice parameter takes place during drying and curing of the mesoporous phase, but two consecutive contractions of 1 and 6% are calculated for the polystyrene extracted and the triblock copolymer extracted crystals, respectively. These blue-shifts are much smaller when silica CVD stabilized samples are employed.

To test the spatial homogeneity of the infiltration process, we have measured the optical reflectance on five different circular spots located along a line having the same length than the whole width of the sample (13 mm) for a colloidal crystal film infiltrated using a dilute solution of the mesoporous precursor. Each spot has an area of 0.1 mm^2 and is 2.5 mm apart from the neighboring ones. The central spot is located approximately at the same position where the 30 μl of the precursor solution were dropped. The filling fraction was then estimated at every spot and for each infiltration cycle by fitting the corresponding spectrum. Because 14 SCI cycles were performed for this experiment, a total of 75 spectra were fitted, including the original ones. A summary of the result of this analysis is shown in Figure 4. Comparison between the results for the different regions allowed us to check the spatial homogeneity of the SCI process as well as its evolution. Results confirm that a similar degree of filling is achieved over the whole sample. The small differences observed ($<5\%$, and much less for the first cycles) seem to be random, although a deeper analysis of the dependence of the filling fraction with the sample features and all the spin-coating parameters is currently being made. It should be noticed that not only does SCI allow an accurate control over the filling fraction, but also prevents the formation of undesired external capping of the film that might modify its optical properties, as it has recently been demonstrated by some of us.[16]

These results show that the mesoporous filling fraction can be experimentally determined by the concentration of the precursor in the dropping solution and the number of infiltration processes performed, although we confirmed that it can also be controlled by the spinning speed. SCI presents major advantages over other colloidal crystal infiltration methods from the liquid phase previously employed.[17,18] It permits an extremely accurate control of the amount of infiltrated material, only comparable to the precision obtained by infiltration by chemical vapor deposition (CVD).[13] In addition, the combination of SCI with spin-coating crystallization techniques recently proposed[19] might allow for the full processing of colloidal photonic crystals by this technique, which is one of the most widely employed in current microelectronics and microphotonics chip technology.

The walls of the spherical cavities present a very low dielectric constant as a result of their high porosity. This low refractive index contrast results in low-intensity Bragg diffractions that, nevertheless, can be clearly observed with the naked eye. Specular reflectance spectra for several hierarchically ordered porous lattices are shown in Figure 5a, demonstrating the control over their photonic crystal properties achievable by varying the sphere template diameter and the degree of infiltrated precursor. Fitting of these spectra was performed introducing the structural features (lattice parameter and filling fraction) obtained from electron microscopy and leaving as variables the optical parameters. By doing so, we found the refractive index of the mesoporous silica skeleton to be $n_{meso} = 1.15$, far below the approximately 1.45 expected for dense silica. Figure 5b and c display pictures of two bimodal porous lattice films as seen from two different angles, clearly showing the angle dependence of the color characteristic of optical diffraction. Both films were obtained from the same polystyrene sphere template, but one of them (bottom sample in both pictures) was previously coated with dense silica.

The two types of hierarchical structures herein presented, stabilized and nonstabilized, should present very different behavior regarding mesopore accessibility. Mesopores in the walls of the *nonstabilized inverted structure* can in principle be accessed much more easily than in standard mesoporous films because of the presence of two nonconnected macroporous lattice. The first one is formed by the large spherical cavities left after the etching of the latex template, and the second one is formed by the interconnected octahedral and tetrahedral pores between the spherical mesoporous shells arranged in a cubic close-packed lattice. In the case of the *stabilized inverted structure*, there should also be an enhancement of the accessibility, but lower than in the case of the nonstabilized one because the dense silica scaffold supporting the mesoporous walls now prevents the entrance from inside of the spherical

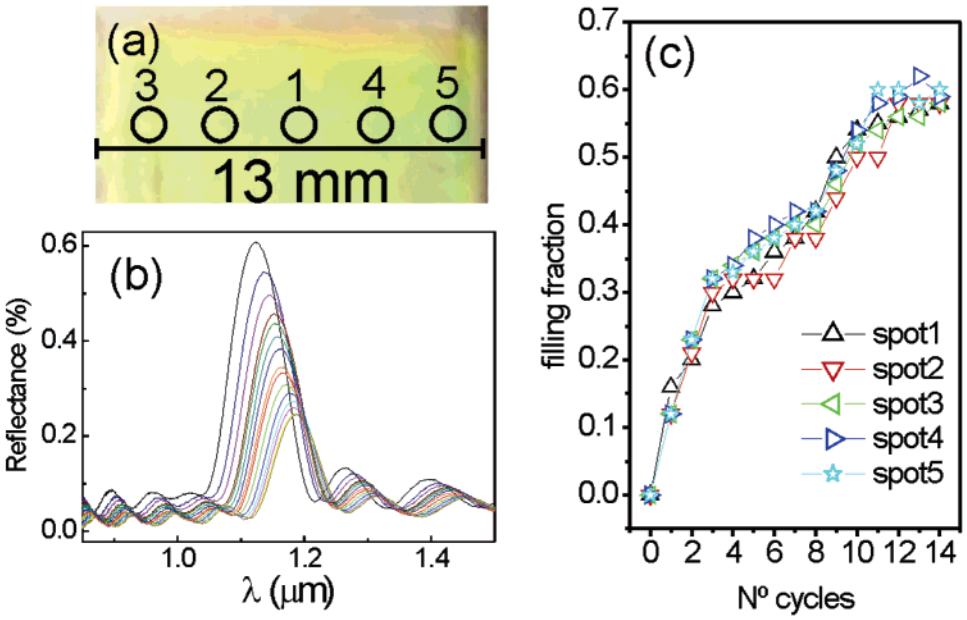

Figure 4. (a) Optical picture of a hierarchically ordered film showing the position of the five different spots (2.5 mm apart one from the other) used for the analysis of the spatial homogeneity of the spin-coating infiltration process. A spatial filter was used to selectively detect light from 0.1 mm^2 circular regions of the sample. (b) A typical series of spectra corresponding to the 14 consecutive SCI cycles performed. In this example, results were obtained measuring on spot 1, which corresponds approximately to the area where the 30 μl of diluted precursor are dropped. (c) Evolution of the filling fraction of the mesoporous phase in the different areas of the sample selected for the analysis. The data have been extracted from the fitting of 75 reflectance spectra.

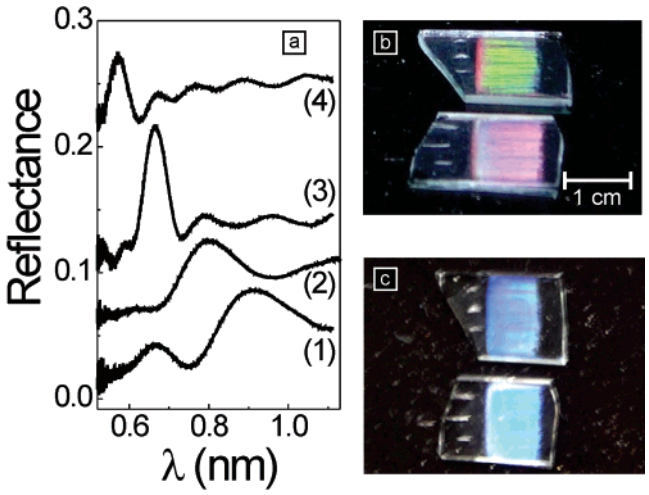

Figure 5. Optical properties of hierarchically ordered bimodal porous silica structures. (a) Specular reflectance spectra of different bimodal films. The incident beam forms an angle of ~0° with respect to the film surface. Spectra (1) and (2) correspond to pure mesoporous shell fcc photonic crystal films obtained from similar polystyrene colloidal crystal film (average sphere diameter 545 nm) after being infiltrated 4 and 3 times, respectively, with the same mesoporous precursor solution. Spectra (3) and (4) correspond to pure mesoporous and mesoporous/dense silica shell photonic crystal films, respectively. Both were obtained from similar templates (average sphere diameter 360 nm). Images in panels (b) and (c) show pictures of the two bimodal porous lattice films whose spectra are labeled as (3) (bottom sample) and (4) (top sample). Pictures were taken collecting the specularly (angle with respect to the film normal ~45°) and backscattered reflected light, respectively.

macropores. Unfortunately, since the seminal works in the field[20] up to the most recent ones,[21] obtaining an estimation of pore size (and therefore accessibility) through mercury or nitrogen adsorption−desorption isotherms remains a challenge[22] because the weight of the sample available for such experiments is below the accepted minimum weight for accurate data to be obtained. Below an acceptable weight of approximately 0.05 g, isotherm data is likely to be erroneous, for the amount of nitrogen adsorbed at each pressure point will be extremely low and outside the range of accuracy of the instrument. In our case, the maximum amount of sample attainable from the films is 0.01 g, so no reliable results can be expected. Scratching several samples to reach the required minimum weight is an option that presents serious drawbacks because pieces of the substrate are usually mixed with the mesoporous film, hence yielding large errors in the sample weight and incorrect results, as has been pointed out before.[23] Several alternative methods have been proposed to overcome the problem of pore size estimation and accessibility in mesoporous films.[23−25] The application of these methods to the new type of mesoporous films herein presented is left as a matter for future research.

Conclusions

We have developed a method to fabricate films of hierarchically ordered porous silica that display optical Bragg diffraction. In that sense, they present a radically new property with respect to the mesoporous films developed up to date. These materials open the opportunity to combine the anomalous light propagation that takes place in photonic crystals with the high mass transport through macropores and high specific surface area, reactivity, and selective separation properties offered by a mesoporous network. We foresee that the interplay of such features might have an impact in fields such as photocatalysis, photochemistry, and chromatography.

Acknowledgment. This work has been funded by Fundación Ramón Areces. I.R. thanks the Spanish Ministry of Science and Technology for a Ramón y Cajal Fellowship.

References and Notes

(1) Antonietti, M.; Bretón, B.; Göltner, C.; Hentze, H. P. *Adv. Mater.* **1998**, *10*, 154.

(2) Mayoral, R.; Requena, J.; Moya, J. S.; López, C.; Cintas, A.; Míguez, H.; Meseguer, F.; Vázquez, L.; Holgado, M.; Blanco, A. *Adv. Mater*. **1997**, *9*, 257.
(3) Joannopoulos, J. D.; Villeneuve, P. R.; Fan, S. *Nature* **1997**, *386*, 143.
(4) Yang, P.; Deng, T.; Zhao, D.; Feng, P.; Pine, D.; Schmelka, B. F.; Whitesides, G. M.; Stucky, G. D. *Science* **1998**, *282*, 2244.
(5) Holland, B. T.; Blanford, C. F.; Do, T.; Stein, A. *Chem. Mater*. **1999**, *11*, 795
(6) Zhou Y, Y.; Antonietti, M. *Chem. Commun.* **2003**, 2564.
(7) Sen, T.; Tiddy, G. J. T.; Casci, J. L.; Anderson, M. W. *Angew. Chem., Int. Ed.* **2003**, *42*, 4649.
(8) Oh, C. G.; Baek, Y.; Ihm, S. K. *Adv. Mater*. **2005**, *17*, 270.
(9) Dong, A. A.; Wang, Y. J.; Tang, Y.; Zhang, Y. H.; Ren, N.; Gao, Z. *Adv. Mater*. **2002**, *14*, 1506.
(10) Yang, S. M.; Ozin, G. A. *Adv. Mater*. **2000**, *12*, 1940.
(11) Yamaguchi, A.; Uejo, F.; Yoda, T.; Uchida, T.; Tanamura, Y.; Yamashita, T.; Teramae, N. *Nat. Mater*. **2004**, *3*, 337.
(12) Bertone, J. F.; Jiang, P.; Hwang, K. S.; Mittleman, D. M.; Colvin, V. L. *Phys. Rev. Lett.* **1999**, *83*, 300.
(13) Míguez, H.; Tetreault, N.; Hatton, B.; Yang, S. M.; Perovic, D.; Ozin, G. A. *Chem. Commun.* **2002**, 2736.
(14) Zhao, D.; Yang, P.; Melosh, N.; Feng, J.; Chmelka, B. F.; Stucky, G. D. *Adv. Mater*. **1998**, *10*, *1380*.
(15) Mittleman, D. M.; Bertone, J. F.; Jiang, P.; Hwang, K. S.; Colvin, V. L. *J. Chem. Phys.* **1999**, *111*, 345.
(16) Mihi, A.; Míguez, H.; Rodríguez, I.; Rubio, S.; Meseguer, F. *Phys. Rev. B* **2005**, *71*, 125131.
(17) Holland, B. T.; Blanford, C. F.; Stein, A. *Science* **1998**, *281*, 538.
(18) Wijnhoven, J. E. G. J.; Vos, W. L. *Science* **1998**, *281*, 802.
(19) Jiang, P.; McFarland, J. *J. Am. Chem. Soc.* **2004**, *126*, 13778.
(20) Yang, H.; Kuperman, A.; Coombs, N.; Mamiche-Afara, S.; Ozin, G. A. *Nature* **1996**, *379*, 703.
(21) Crepaldi, E. L.; Soler-Illia, G. J. A. A.; Grosso, D.; Cagnol, F.; Ribot, F.; Sanchez, C. *J. Am. Chem. Soc.* **2003**, *125*, 9770.
(22) Ayral, A.; El Mansouri, A.; Vieira, M. P.; Pilon, C. *J. Mater. Sci. Lett.* **1998**, *17*, 883.
(23) Nossov, A.; Haddad, E.; Guenneau, F.; Mignon, C.; Gédéon, A.; Grosso, D.; Babonneau, F.; Bonhomme, C.; Sanchez, C. *Chem. Commun.* **2003**, 2476.
(24) Dull, T. L.; Frieze, W. E.; Gidley, D. W. Sun, J. N.; Yee, A. F. *J. Phys. Chem. B* **2001**, *105*, 4657.
(25) Baklanov, M. R.; Mogilnikov, K. P.; Polovinkin, V. G.; Cultsev, F. N. *J. Vac. Sci. Technol.* **2000**, *18*, 1385.